DOI:10.1021/jf102501n

JOURNAL OF AGRICULTURAL AND FOOD CHEMISTRY
ARTICLE

Design of a Multifunctional Nanohybrid System of the Phytohormone Gibberellic Acid Using an Inorganic Layered Double-Hydroxide Material

Inas H. Hafez,[†] Mohamed R. Berber,*[,†] Keiji Minagawa,[†] Takeshi Mori,[‡] and Masami Tanaka[§]

[†]Institute of Technology and Science, The University of Tokushima, Tokushima 770-8506, Japan, [‡]Department of Applied Chemistry, Kyushu University, Fukuoka 819-0395, Japan, and [§]Faculty of Pharmaceutical Sciences, Tokushima Bunri University, Tokushima 770-8514, Japan

To offer a multifunctional and applicable system of the high-value biotechnological phytohormone gibberellic acid (GA), a nanohybrid system of GA using the inorganic Mg−Al layered double-hydroxide material (LDH) was formulated. The ion-exchange technique of LDH was applied to synthesize the GA−LDH hybrid. The hybrid structure of GA−LDH was confirmed by different spectroscopic techniques. The nanohybrid size was described by SEM to be ∼0.1 μm. The GA−LDH nanohybrid structure was the key parameter that controlled GA properties. The layered molecular structure of LDH limited the interaction of GA molecules in two-dimensional directions. Accordingly, GA molecules did not crystallize and were released in an amorphous form suitable for dissolution. At various simulated soil solutions, the nanohybrids showed a sustained release process following Higuchi kinetics. The biodegradation process of the intercalated GA showed an extended period of soil preservation as well as a slow rate of degradation.

KEYWORDS: Gibberellic acid; LDH; safe preservation; release kinetics; degradation

INTRODUCTION

Growth and development of plants from stem elongation to the ripening of fruit is controlled by internal chemical signals called plant growth regulators. Gibberellins (GAs) are a group of diterpenoid acids that function as plant growth regulators. They influence a wide range of developmental processes in higher plants. One GA is gibberellic acid (GA). GA is an important biotechnological plant phytohormone with various applications in agriculture, viticulture, gardens, and horticulture (*1*). The effects of GA depend on its concentration as well as its application method. Generally, GA is applied to commercial crops by foliar spraying, and in some instances it is preferable to add it directly to the soil (*2*). With respect to foliar spraying of GA, for example, treatment of *Catharanthus roseus* resulted in changes in leaf morphology and an increase in stem elongation, leaf and internode length, and plant height (*3*). Also, the spray of GA on mustard (*Brassica juncea* L. Czern & Coss.) enhanced plant dry mass, leaf area, carbon dioxide exchange rate, and plant growth rate and significantly improved nitrogen-use efficiency through redistribution of nitrogen to seeds (*4*).

However GA has low water solubility and rapidly decomposes by soil micro-organisms (*5*). Thus, soil-applied GA strongly depends on both GA absorption and biodegradation rate. Additionally, uncontrolled doses of GA can cause an herbicidic-like effect that in some cases destroys the plant (*6*). Driven by the mentioned GA application problems and its biological significance, there is a need in the art of advanced formulation systems to offer a safe preservation of GA biodegradation and to maintain controlled release doses into the applied soil.

Inorganic matrices, such as layered double hydroxides (LDHs), are receiving much attention in the development of new and more effective formulation systems of bioactive materials (*7*). LDHs consist of layers of M^{2+} hydroxide with M^{3+} isomorphically substituted to give the layers a net positive charge. This charge is balanced by interlayer hydrated anions that can be easily exchanged by beneficial organic anions (*8*, *9*). These materials offer many benefits across a wide range of industrial applications. In pharmacy, drug−LDH nanocomposites were formulated to control the amount of drug released, drug solubility, and drug dissolution rate (*10*−*14*). In addition, the intercalation of bioactive compounds such as vitamins and nucleic acids (*15*, *16*) into LDH offered a safe preservation of the guest bioactivity without any deterioration of the structural integrity. In agriculture, LDH nanocomposite formulations controlled the herbicidal efficiency of acid herbicides (*17*) and also minimized the losses of plant pesticides (*18*). Thus, we envision that the strategy of using LDH nanoformulation will hold promise as a versatile platform for GA low solubility, preservation, and controlled release properties as well as the GA biodegradation process.

We therefore undertook the synthesis and characterization of a nanohybrid formulation system of GA using a Mg−Al LDH inorganic matrix. Following the intercalation process, we subsequently studied the release properties of the nanohybrid at

*Corresponding author (phone +81-88-656-9153; fax +81-88-655-7025; e-mail mrberber@sy34.chem.tokushima-u.ac.jp).

 Published on Web 08/19/2010

various simulated soil solutions, as well as the degradation behavior in different soils to evaluate the effect of LDH on GA properties after the intercalation process.

MATERIALS AND METHODS

Materials. Magnesium nitrate hexahydrate, aluminum nitrate nanohydrate, (purity = 99.5 and 98%, respectively; Wako Pure Chemical Industries, Ltd.) and gibberellic acid (purity ≥ 90%; ACROS Organics, Ltd.) were used as received. All solutions were prepared using deionized water (18.2 MΩ/cm, produced from Milli-Q Grandient ZMQG000kt).

Coprecipitation Technique of NO_3−LDH. To a 200 mL three-necked round flask containing 30 mL of 1.0 M sodium nitrate solution was added dropwise a 50 mL solution of 8.538 g (0.0333 M) of magnesium nitrate hexahydrate and 6.249 g (0.01666 M) of aluminum nitrate nanohydrate (metal ion molar ratio of Mg^{2+}/Al^{3+} = 2) with constant magnetic stirring. During the metal ion addition, the pH of the suspension was kept constant at 8.0 by adding appropriate amounts of 2.0 M NaOH solution. The final volume of the preparation medium was augmented to 100 mL by deionized water. The resultant suspension was stirred at 70 °C for 24 h under N_2 flow. At the end of the reaction, the formed Mg−Al LDH material was collected by filtration (0.45 μm Millipore membrane), washed several times with deionized water, and finally freeze-dried.

Nanohybrid Synthesis of GA−LDH by Anion-Exchange Technique. In a 100 mL round flask was dissolved 2.0 g of GA in 100 mL of deionized water by adjusting the solution pH to 8.0 using 2.0 M NaOH solution. To the GA solution was added 1.0 g of NO_3−LDH with constant stirring. The reaction mixture was stirred at 40 °C for 7 days. After the reaction, the obtained GA−LDH material was collected by filtration (0.45 μm Millipore membrane) and washed several times by 0.1 M NaOH solution and subsequently deionized water until a negative test was obtained for GA in the washing medium. A UV spectrophotometer (U-3210, Hitachi, Japan) was used to check for the presence of GA in the washing medium at 254 nm (*5*). Finally, the collected GA−LDH was freeze-dried.

Determination of GA Loading. The amount of GA loaded into LDH was calculated by using a UV quantitative method as follows. A known amount of the nanohybrid was dissolved in 10 mL of 1.0 M HCl. The obtained solution was diluted using a phosphate buffer of pH 7.4. The GA concentration was determined from the absorption peak at 254 nm. The GA ratio was expressed by the percentage of GA weight intercalated in a unit weight of nanohybrid. The UV method was also used to check the integrity of GA after the intercalation process.

GA Release Measurements. The dissolution of GA and GA−LDH nanohybrid was monitored in the following buffer mediums: buffer A as a simulated acidic soil solution (a 100 mL solution mixture of the same volumes of 0.25 mM KCl, 1.0 mM $MgCl_2$, and 5.0 mM $CaCl_2$; a few drops of 10.0 mM HCl solution was used to adjust the solution pH at 3.0) and buffer B as a simulated normal soil solution (a 100 mL solution mixture of the same volumes of 0.25 mM KCl, 1.0 mM $MgCl_2$, and 5.0 mM $CaCl_2$; a few drops of 10.0 mM NaOH solution was used to adjust the solution pH at 7.0). The anionic buffer composition was defined on the basis of literature data (*19*, *20*). The release experiment was performed as follows: In a round-bottom flask, a sample of 100 mg of GA or 250 mg of GA−LDH nanohybrid was dispersed in 100 mL of buffer solution, which was maintained at 25.0 ± 0.1 °C with constant agitation. At appropriate time intervals, a 1.0 mL sample solution was withdrawn from the release medium and filtered by using a 0.45 μm Millipore filter unit to remove the insoluble particles. The filtrate was diluted and assayed for UV measurement at 254.0 nm. The removed aliquot was immediately replenished by the same volume of the used buffer, which was equilibrated at the same reaction temperature (*21*). The dissolution experiment of each sample in each buffer was performed in triplicates.

Degradation Process of GA. To investigate the effect of LDH on the degradation behavior of GA, two different cultivated soils varying in texture and physicochemical properties were used. Soil A, located at the Agricultural Research Institute, Ishii, Tokushima prefecture, Japan (latitude 34° 03′ N and longitude 134° 26′ E), was a sandy soil; its texture analysis yielded an average of 90% sand, 2% silt, and 8% clay. Soil B, located at the University of Tokushima, Japan (latitude 34° 04′ N and longitude 134° 33′ E) was a sandy clay loam soil with an average of 52% sand, 13% silt, and 35% clay. The pH, EC, C/N, and organic matter ratio were 5.05, 0.11 ds/m, 3.0%, and 0.8% for soil A, whereas they were 7.10, 0.41 ds/m, 12.4%, and 4.3% for soil B, respectively.

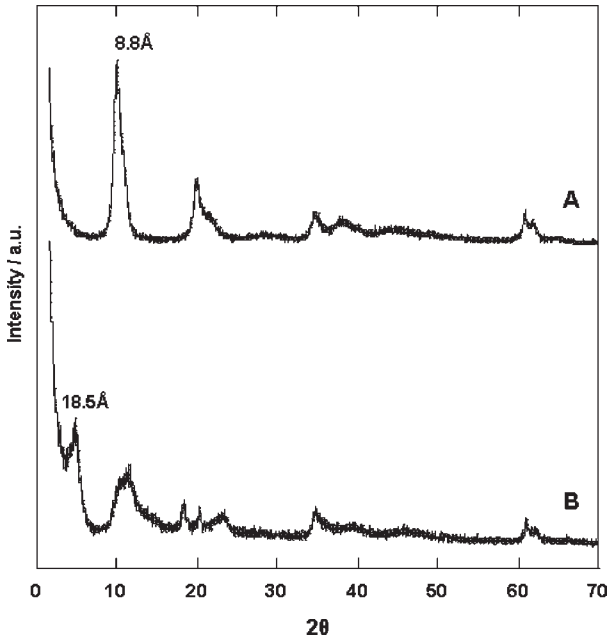

Figure 1. X-ray diffraction patterns of NO_3−LDH (**A**) and GA−LDH (**B**).

The degradation process was performed as follows: 100 mg of GA was mixed throughout 500 g of soil A, which had a relative humidity of ∼65%. The GA−soil mixture was incubated aerobically in the dark at 25 ± 1.0 °C. At different time intervals, a 50 g mixture was extracted twice by vigorous shaking for 1.0 h, using each time 100 mL of 0.1 M phosphate buffer (pH 7.4). The two extractions were collected together, and then the amount of the extracted GA was determined by a UV spectrophotometer at 254 nm. By the same procedure the degradation of GA in soil B and the degradation of GA−LDH in soils A and B were investigated (in the case of GA−LDH nanohybrid, 250 mg of GA-LDH was mixed with 500 g of soil). The degradation process of each sample in each soil was performed in triplicates.

Characterization. X-ray powder diffraction patterns were recorded on a Rigaku X-ray diffractometer using CuKα radiation at λ = 1.5405 Å. The measurement was performed in the 2θ range 1.5−70° with a 2θ scanning step of 0.02°, a scanning step time of 5 s, a filament intensity of 40 mA, and a voltage of 150 kV. Infrared spectra (KBr disk method) were recorded on a Bio-Rad FTS 3000MX FT-IR spectrophotometer with a TGS detector in the wavenumber range of 4000−500 cm^{-1} by accumulating 16 scans at 4 cm^{-1} resolution. Thermogravimetric analysis (TGA) was conducted with a Shimadzu thermogravimetric analyzer (TGA-50, TA-60WS) using a platinum cell with a heating rate of 10 °C/min, under a N_2 flow of 20 mL/min. The scanning electron micrographs (SEM) were captured by a Hitachi FE-SEM S-4700 microscope. The soil organic matter was measured by following the method described in the literature (*22*).

RESULTS AND DISCUSSION

X-ray Powder Diffraction. Figure 1 shows the XRD patterns of LDH and the GA−LDH nanohybrid. Pattern **A** indicates the formation of the NO_3 form of LDH with sharp and symmetric (*00l*) reflections. Using Bragg's law ($n\lambda = 2d \sin\theta$), the basal *d*-spacing was calculated to be 8.8 Å, similar to previous data (*23*). As a result of intercalation of GA, the basal *d*-spacing was expanded to 18.5 Å (pattern **B**). The GA−LDH nanohybrid interlayer distance was calculated by subtracting the inorganic layer thickness (4.8 Å) (*24*) from the d_{003}-spacing. The determined value (13.7 Å) was larger than GA molecular widths (8.3 Å) and lower than GA molecular length (14.0 Å). However, LDH attaches its interlayer anions through an electrostatic interaction (*8*). Thus, we speculated that GA molecules were stacked into

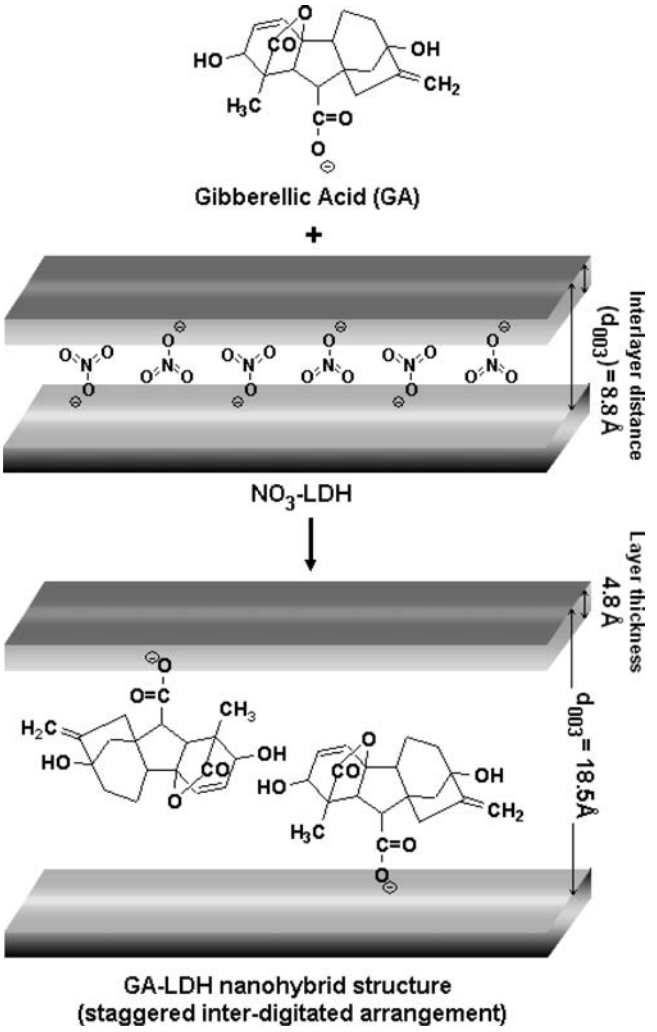

Figure 2. Systematic diagram of GA−LDH intercalation process.

LDH as a monolayer of a staggered interdigitated arrangement through the attachment of GA carboxyl groups with the LDH positive layers, as schematically drawn in **Figure 2**.

Fourier Transform Infrared (FT-IR) Spectroscopy. FT-IR spectra were measured to obtain further information about the nanohybrid molecular structure. **Figure 3A** shows that the characteristic peaks of NO_3−LDH, the asymmetric stretching band of the interlayer nitrate (ν_{NO3}) and the hydroxyl group stretching vibration band (ν_{OH}) of LDH layers, were observed at 1366 and 3450 cm^{-1}, respectively (*23*). The lattice vibration modes (ν_{M-O}) were detected at 770, 640, and 555 cm^{-1} (*25*). The FT-IR spectra of GA (**Figure 3B**) showed complex features below 1500 cm^{-1}, which can be attributed to the bending and stretching of aromatic rings, alcohols, and carbonyl bonds. The stretching vibration band of COOH group was detected at 1742 cm^{-1}. The weak stretching vibration modes of GA alkyl groups (ν_{C-H}) were detected between 3050 and 2860 cm^{-1}. As a result of intercalation of GA into LDH (**Figure 3C**), new peaks emerged such as symmetric and asymmetric modes of COO^- at 1560 and 1670 cm^{-1}, respectively, besides the characteristic peaks of GA and LDH. This information indicated that GA molecules were combined with LDH layers through electrostatic interactions.

Structure Morphology. Figure 4 displays the SEM images of the synthesized materials. Image **A** shows a regular hexagonal platelet structure characteristic for LDH particles. The regularity of the LDH particles confirmed the good crystallinity recorded by X-ray measurement. In the case of GA−LDH

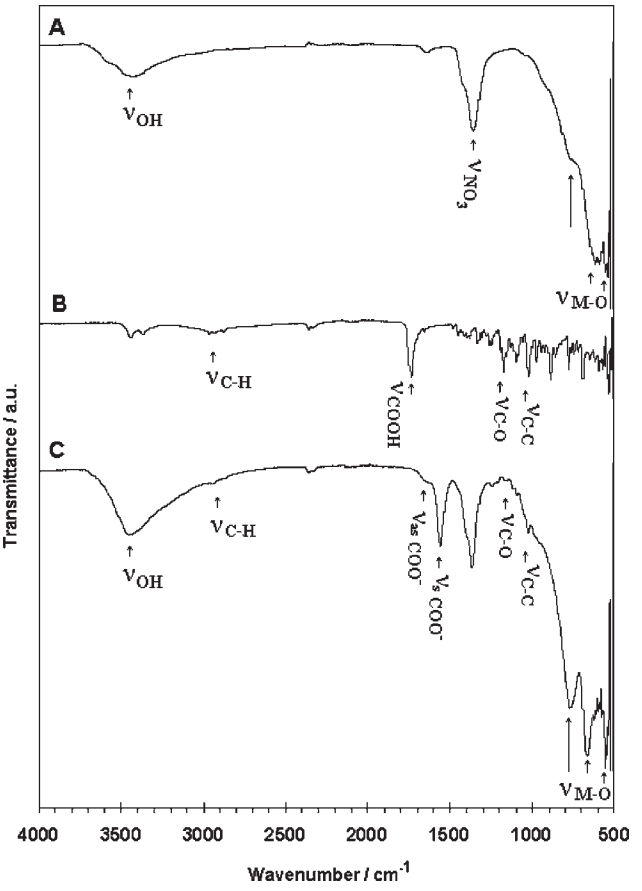

Figure 3. Infrared spectra of LDH (**A**), GA (**B**), and GA−LDH (**C**).

(image **B**), such regular structure was demolished, and aggregates composed of small particles (diameter ~ 0.1 μm) were observed. This aggregation process was probably due to the hydrophobic interaction of the LDH surface-adsorbed GA particles. Conclusively, the nanohybrid structure of GA−LDH was confirmed by SEM.

Thermal Stability of GA−LDH Nanohybrids. TGA and differential thermal analysis curves of LDH, GA, and GA−LDH nanohybrids are shown in **Figure 5**. In the case of LDH (**Figure 5A**), the weight loss was observed to proceed mainly in three steps: 10% from 90 to 160 °C (the loss of the physically adsorbed water molecules), 6% from 170 to 250 °C (the loss of the interlayer water molecules), and 31% from 250 to 570 °C (the dehydroxylation process and the decomposition of the interlayer anions) (*26*). After the intercalation of GA into LDH, the TGA curve was significantly changed (**Figure 5C**). The amount of interlayer water was decreased to be 4% (probably due to the hydrophobic nature of the intercalated GA). The overall weight loss was increased to 66%. The onset temperature of decomposition shifted to a higher value. Accordingly, the stability of GA was promoted against the thermal decomposition after the nanohybrid formation.

Controlled Release and Dissolution of GA Nanohybrids. The nanohybrid loading ratio of GA was estimated to be 40%. For a good comparison of GA dissolution before and after the intercalation process, the loading ratio of GA was taken into consideration during the release experiments.

Insets to panels **A** and **B** of **Figure 6** show the solubility of pure GA in the studied buffer media A and B, respectively. The determined solubility values after 24 h of dissolution were very small (45 mg/L in buffer A and 104 mg/L in buffer B). The low solubility of GA in both buffers A and B was related to the acidic

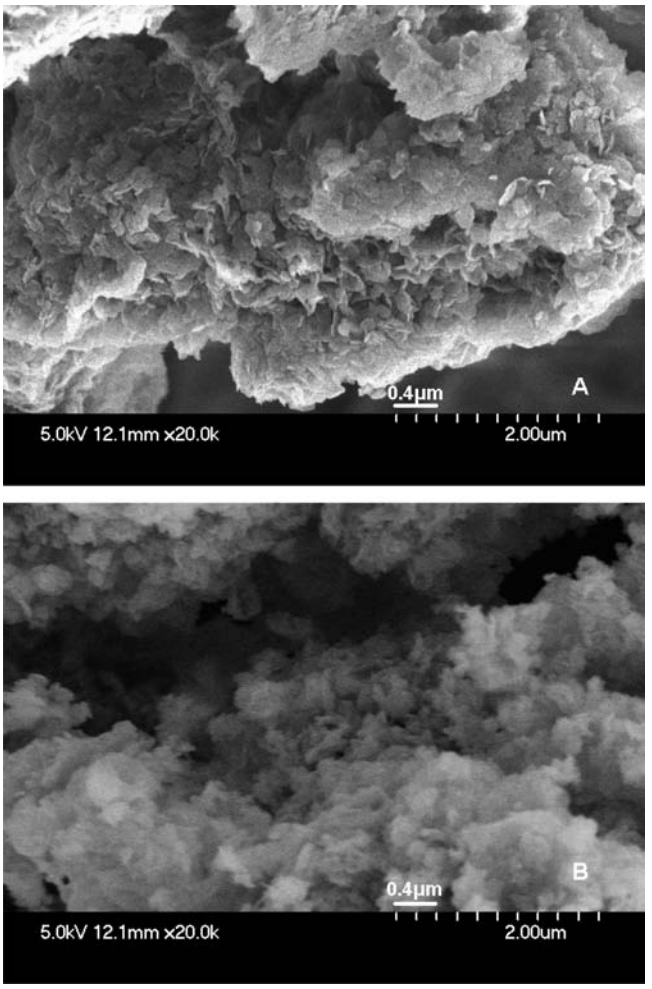

Figure 4. SEM images of LDH (**A**) and GA−LDH (**B**).

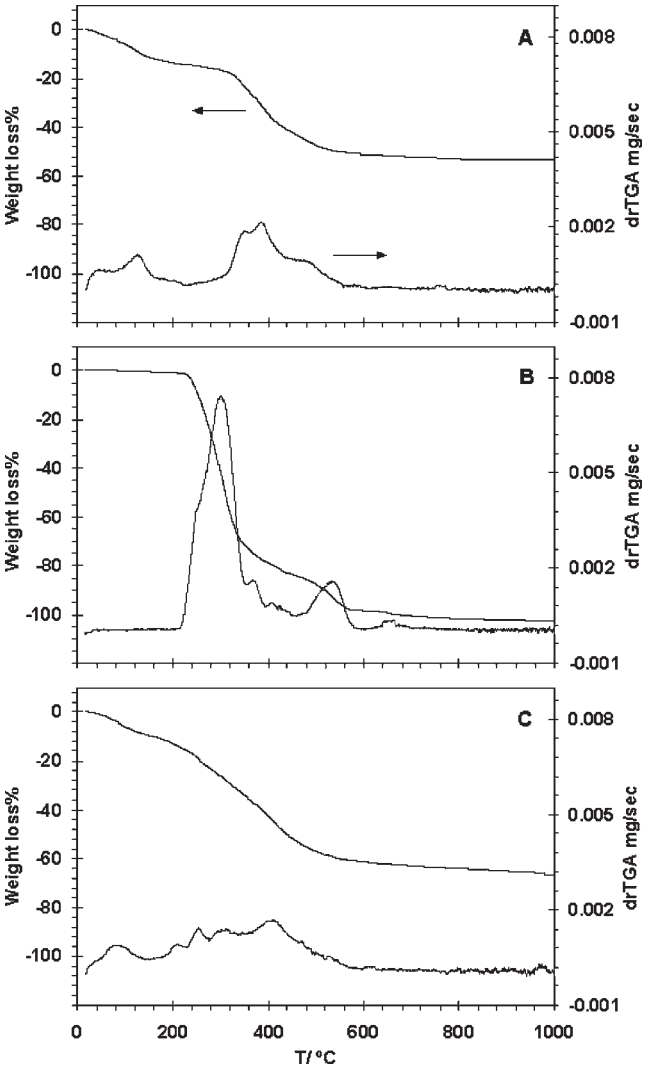

Figure 5. Thermogravimetric analysis and differential curves of LDH (**A**), GA (**B**), and GA−LDH (**C**).

character and the high crystallinity of GA. Such dissolution data indicated that GA cannot achieve its desired role as a plant growth regulator in a long-term soil application.

After the nanohybrid formation of GA−LDH, the release profile changed and showed a controlled release process of GA with time in different buffer media (**Figure 6**). During the first 24 h, around 800 mg/L (80%) and 600 mg/L (60%) of the intercalated GA were released in buffers A and B, respectively. The release of GA from the nanohybrids continued after that in a sustained manner until reaching near equilibrium after 6 days with a 90% release in buffer A and an 80% release in buffer B. The new GA−LDH nanohybrid structure was the key parameter that controlled the release properties of the intercalated GA. The layered structure of LDH limited the interaction of GA in two-dimensional directions. Accordingly, GA molecules were prevented from crystallization and released in an amorphous form suitable for dissolution. Moreover, the anion exchange mechanism of LDH (*27*) modified the release profile of GA. The phase boundary formed between the internal zone (GA−LDH, large *d*-spacing) and the external zone (exchanged LDH, small *d*-spacing) lowered the amount of GA released with time.

GA Release Kinetics and Mechanism. To study the release kinetics of GA−LDH nanohybrid, the release data were investigated at various kinetic models: zero order as a cumulative amount of GA released versus time, first order (eq 1) as ln cumulative percentage of drug remaining versus time, and Higuchi's model (eq 2) (*28*, *29*), which describes the release from an insoluble matrix as a cumulative percentage of drug released versus square root of time.

$$\ln(C_i - C_t) = \ln C_i - kt \quad (1)$$

where C_t is the amount (mg) of GA released at time t, C_i is the amount (mg) of GA intercalated into LDH, and k is the first-order rate constant.

$$Q_t = kt^{0.5} \quad (2)$$

where Q_t is the amount (mg) of GA released at time t and k is the release rate constant of the Higuchi model.

The zero-order kinetics did not match at all the experimental release data. The first-order model did not fit well the whole range of the release data; only the release of the first 12 h was in some agreement with the first-order kinetics (**Figure 7A**). The plot of Q_t against $t^{0.5}$ (**Figure 7B**, Higuchi kinetics) was in good agreement with the experimental release data of GA−LDH, and it supported the understanding of the GA−LDH release mechanism. As seen from **Figure 7B**, the plot showed a variation of gradient with high linearity (R^2) at different release times. This means that the release of GA from the LDH matrix occurred in more than one step. The first instantaneous release step seemed to be the physically adsorbed GA on the external surface of LDH.

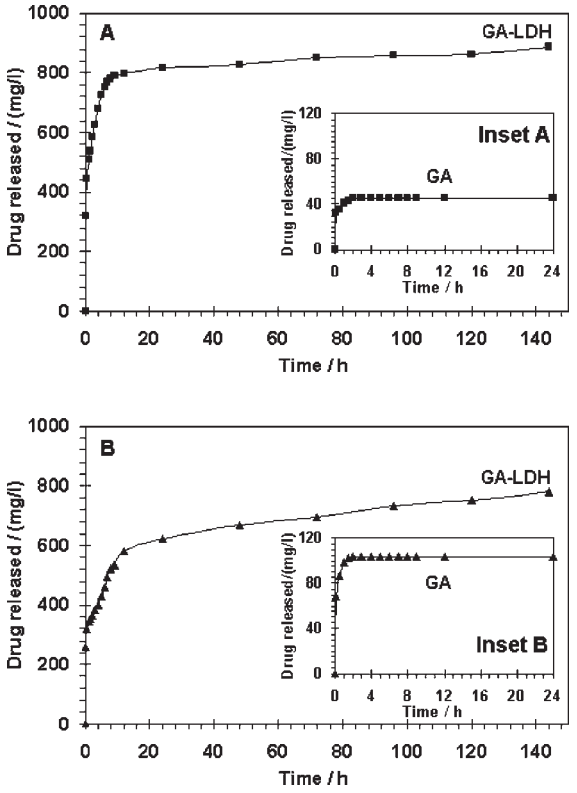

Figure 6. Release profile of GA−LDH and pure GA (inset) in buffer A (**A**) and in buffer B (**B**).

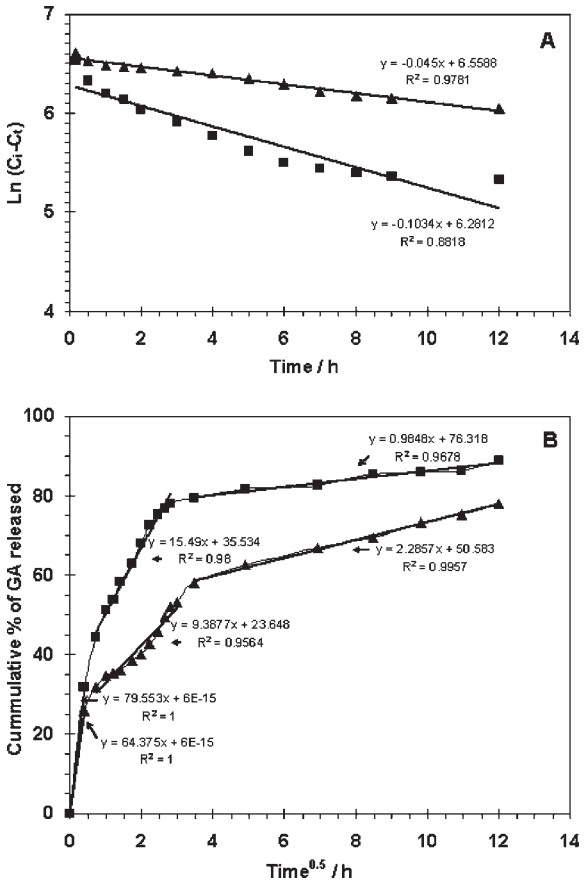

Figure 7. Release kinetics of GA−LDH nanohybrid of first-order model (**A**) and Higuchi model (**B**) in buffer A (■) and in buffer B (▲).

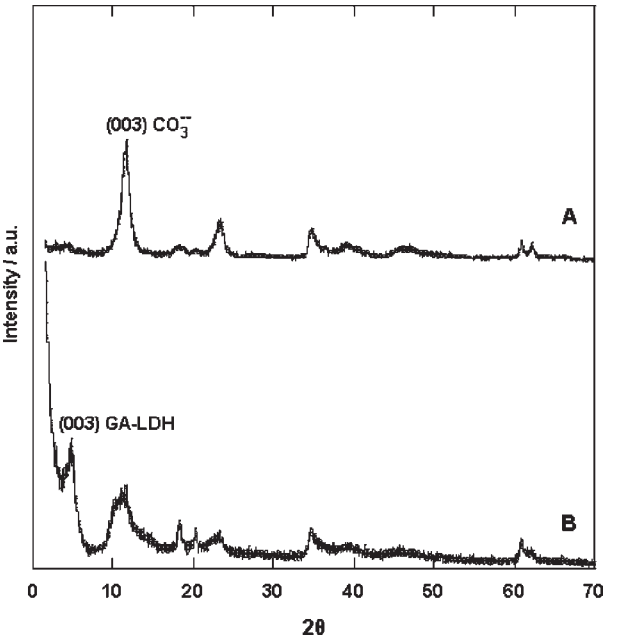

Figure 8. X-ray diffraction patterns of the residue of the releasing medium B (**A**) and GA−LDH before release (**B**).

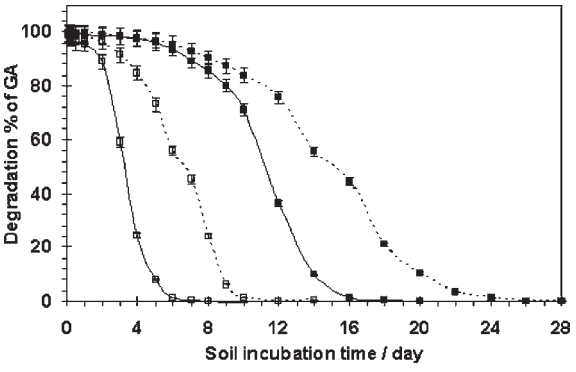

Figure 9. GA degradation dependence of incubation time in soil A (dashed line) and soil B (solid line) before intercalation (□) and after intercalation (■).

The second steeper release region was caused by the anion-exchange process of the intercalated GA, because the release of LDH interlayer particles is a rate-controlling step depending on the exchange of the medium's anions. The third region of the plot corresponded to the equilibrium stage of the release process. This region showed a slow rate of GA exchange. The regression of the exchange rate was due to the phase boundary formed into LDH during the anion-exchange process (*27*).

Figure 8 confirms the anion-exchange process of GA. The XRD pattern of GA−LDH residue of the dissolution medium B (**Figure 8A**) showed a regression in the characteristic peaks of GA−LDH and a progression of the exchanging anion peaks.

Degradation Process of GA. Figure 9 shows the biodegradation behavior of GA as a function of soil incubation time. Before the intercalation process, GA started to degrade after 1 day of incubation in soil B and after 2 days in soil A. The degradation process was fast in both soils, because GA completely disappeared from soil B after 6 days and from soil A after 10 days. The rapid degradation of GA in soil B compared to soil A was probably due to the texture of the soils, as the high percentage of organic matter in soil B supports a good environment for the activity of micro-organisms (*30*).

After the intercalation process, a significant protective role of LDH against the biodegradation of GA was observed. During the first 5 days of nanohybrid soil incubation, there was no noticeable change in the degradation of GA in both soils A and B. Gradual degradations of 15 and 25% of GA in soils A and B, respectively, were noted during the next 5 days. The gradual degradation continued over 20 days of incubation in soil B and over 28 days in soil A. Accordingly, LDH nanohybrid formulation offered a sustained biodegradation process by safe preservation of GA against soil micro-organisms.

Specifically, this work introduced a new nanohybrid system of an important biotechnological plant growth phytohormone (GA). The strategy of using LDH nanoformulation offered a multifunctional platform for GA low solubility, preservation, biodegradation, and controlled release properties. Long-term soil application of the high-value GA was supported by an extended period of preservation into LDH and a slow rate of degradation.

ABBREVIATIONS USED

GA, gibberellic acid; LDH, layered double hydroxide; EC, electrical conductivity; C/N, carbon/nitrogen ratio.

ACKNOWLEDGMENT

We acknowledge the Agricultural Research Institute, Ishii, Japan for supporting us with soil and information. Also, we express our sincere appreciation and deepest gratitude to Dr. Tomohiro Hirano in our department for his kind assistance through the progress of the work.

LITERATURE CITED

(1) Bandelier, S.; Renaud, R.; Durand, A. Production of gibberellic acid by fed-batch solid state fermentation in an aseptic pilot-scale reactor. *Process Biochem*. **1997**, *32*, 141–145.

(2) De Souza, I. R. P.; MacAdam, J. W. Gibberellic acid and dwarfism effects on the growth dynamics of B73 maize (*Zea mays* L.) leaf blades: A transient increase in the apoplastic peroxidase activity precedes cessation of cells elongation. *J. Exp. Bot*. **2001**, *52*, 1673–1682.

(3) Srivastava, N. K.; Srivastava, A. K. Influence of gibberellic acid on $^{14}CO_2$ metabolism, growth, and production of alkaloids in *Catharanthus roseus*. *Photosynthetica* **2007**, *45*, 156–160.

(4) Khan, N. A.; Mir, R.; Khan, M.; Javid, S.; Samiullah Effects of gibberellic acid spray on nitrogen yield efficiency of mustard grown with different nitrogen levels. *Plant Growth Regul*. **2002**, *38*, 243–247.

(5) Anderson, S. J.; Franco-Vizcaino, E.; Jarrel, W. M. Dwarf pea response to gibberellic acid applied to soil through a drip irrigation system, and gibberellic acid biodegradation in soil. *Plant Soil* **1988**, *112*, 289–292.

(6) Tsatsakis, A. M.; Shtilman, M. I. Polymeric derivatives of plant growth regulators: synthesis and properties. *Plant Growth Regul*. **1994**, *14*, 69–77.

(7) Berber, M. R.; Hafez, I. H.; Minagawa, K.; Mori, T.; Tanaka, M. Nanocomposite formulation system of lipid-regulating drugs based on layered double hydroxide: Synthesis, characterization and drug release properties. *Pharm. Res*. **2010**, DOI: 10.1007/s11095-010-0175-x.

(8) Costantino, U.; Marmottini, F.; Nocchetti, M.; Vivani, R. New synthetic routes to hydrotalcite-like compounds: characterisation and properties of the obtained materials. *Eur. J. Inorg. Chem*. **1998**, 1439–1446.

(9) Ogawa, M.; Kaiho, H. Homogeneous precipitation of uniform hydrotalcite particles. *Langmuir* **2002**, *18*, 4240–4242.

(10) Darder, M.; Blanco, M. L.; Aranda, P.; Leroux, F.; Hitzky, E. R. Bio-nanocomposites based on layered double hydroxides. *Chem. Mater*. **2005**, *17*, 1969–1977.

(11) Li, B.; He, J.; Evans, D. G.; Duan, X. Enteric-coated layered double hydroxides as a controlled release drug delivery system. *Int. J. Pharm*. **2004**, *287*, 89–95.

(12) Tronto, J.; Reis, M. J.; Silvério, F.; Balbo, V. R.; Marchetti, J. M.; Valim, J. B. In vitro release of citrate anions intercalated in magnesium aluminum layered double hydroxides. *J. Phys. Chem*. **2004**, *65*, 475–480.

(13) Bingxin, L.; Jing, H.; Evans, D. G.; Xue, D. Inorganic layered double hydroxides as a drug delivery system: Intercalation and in vitro release of fenbufen. *Appl. Clay Sci*. **2004**, *27*, 199–207.

(14) Berber, M. R.; Minagawa, K.; Katoh, M.; Mori, T.; Tanaka, M. Nanocomposites of 2-arylpropionic acid drugs based on Mg−Al layered double hydroxide for dissolution enchancement. *Eur. J. Pharm. Sci*. **2008**, *35*, 354–360.

(15) Aisawa, S.; Higashiyama, N.; Takahashi, S.; Hirahara, H.; Ikematsu, D.; Kondo, H.; Nakayama, H.; Narita, E. Intercalation behavior of L-ascorbic acid into layered double hydroxides. *Appl. Clay Sci*. **2007**, *35*, 146–154.

(16) Sokolova, V.; Epple, M. Inorganic nanoparticles as carriers of nucleic acids into cells. *Angew. Chem., Int. Ed*. **2008**, *47*, 1382–1395.

(17) Cardoso, L. P.; Celis, R.; Cornejo, J.; Valim, J. B. Layered double hydroxides as supports for the slow release of acid herbicides. *J. Agric. Food Chem*. **2006**, *54*, 5968–5975.

(18) El-Nahhal, Y.; Undabeytia, T.; Polubesova, T.; Mishael, Y. G.; Nir, S.; Rubin, B. Organo-clay formulations of pesticides: reduced leaching and photodegradation. *Appl. Clay Sci*. **2001**, *18*, 309–326.

(19) Baker, D. E. A new approach to soil testing. II. Ionic equilibria involving H, K, Ca, Mg, Mn, Fe, Cu, Zn, Na, P and S. *Soil Sci. Soc. Am. J*. **1973**, *37*, 537–541.

(20) Park, M.; Komarneni, S. Ammonium nitrate occlusion vs. nitrate ion exchange in natural zeolites. *Soil Sci. Soc. Am. J*. **1998**, *62*, 1455–1459.

(21) Halder, A.; Sa, B. Preparation and in vitro evaluation of polystyrene-coated diltiazem-resin complex by oil-in-water emulsion solvent evaporation method *AAPS PharmSciTech* **2006**, 7, article 46.

(22) Miall, S.; Miall, L. M. Analysis of soil and compost. In *Methods in Agricultural Chemical Analysis*; Faithfull, N. T., Ed.; CABI Publishing: Wallingford, U.K., 2002; pp 78.

(23) Olanrewaju, J.; Newalkar, B. L.; Mancino, C.; Komarneni, S. Simplified synthesis of nitrate form of layered double hydroxide. *Mater. Lett*. **2000**, *45*, 307–310.

(24) Miyata, S. The syntheses of hydrotalcite-like compounds and their structures and physico-chemical properties-I: the systems Mg^{2+}−Al^{3+}−NO_3^-, Mg^{2+}−Al^{3+}−Cl^-, Mg^{2+}−Al^{3+}−ClO_4^-, Ni^{2+}−Al^{3+}−Cl^- and Zn^{2+}−Al^{3+}−Cl^-. *Clays Clay Miner*. **1975**, *23*, 369–370.

(25) Lin, Y.; Wang, J.; Evans, D. G.; Li, D. Layered and intercalated hydrotalcite-like materials as thermal stabilizers in PVC resin. *J. Phys. Chem. Solids* **2006**, *67*, 998–1001.

(26) Labajos, F. M.; Rives, V.; Ulibarri, M. A. Effect of hydrothermal and thermal treatments on the physicochemical properties of Mg−Al hydrotalcite-like materials. *J. Mater. Sci*. **1992**, *27*, 1546–1552.

(27) Kaneyoshi, M.; Jones, W. Exchange of interlayer terephthalate anions from a Mg−Al layered double hydroxide: formation of intermediate interstratified phases. *Chem. Phys. Lett*. **1998**, *296*, 183–187.

(28) Higuchi, T. Mechanism of sustained action medication: theoretical analysis of rate of release of solid drugs dispersed in solid matrices. *J. Pharm. Sci*. **1963**, *52*, 1145–1149.

(29) Gohel, M. C.; Panchal, M. K.; Jogani, V. V. Novel mathematical method for quantitative expression of deviation from the Higuchi model. *AAPS PharmSciTech* **2000**, 1, article 31.

(30) Willems, H. P. L.; Lewis, K. J.; Dyson, J. S.; Lewis, F. J. Mineralization of 2,4-D and atrazine in the unsaturated zone of a sandy loam soil. *Soil Biol. Biochem*. **1996**, *28*, 989–996.

Received for review June 29, 2010. Revised manuscript received August 8, 2010. Accepted August 9, 2010.